RSC Advances

PAPER

View Article Online
View Journal | View Issue

Cite this: *RSC Adv.*, 2018, **8**, 36407

Coupled magnetic–elastic and metal–insulator transition in epitaxially strained $SrMnO_3/BaMnO_3$ superlattices

Jin-Feng Wang, *[a] Zheng Li,[a] Zhao-Tong Zhuang,[a] Yan-Ming Zhang[a] and Jun-Ting Zhang[b]

Received 5th July 2018
Accepted 13th October 2018

DOI: 10.1039/c8ra05737k

rsc.li/rsc-advances

The spin–phonon coupling and the effects of strain on the ground-state phases of artificial $SrMnO_3/BaMnO_3$ superlattices were systematically investigated using first-principles calculations. The results confirm that this system has antiferromagnetic order and an intrinsic ferroelectric polarisation with the *P4mm* space group. A tensile epitaxial strain can drive the ground state to another antiferromagnetic–ferroelectric phase and then to a ferromagnetic–ferroelectric phase with the *Amm2* space group, accompanied by a change in the ferroelectric polarisation from an out-of-plane direction to an in-plane direction. In contrast, a compressive strain could induce a transition from the antiferromagnetic insulator phase to the ferromagnetic metal phase.

I. Introduction

Recently, remarkably rich strongly correlated electronic behaviours have been discovered at perovskite oxide interfaces or in thin films, such as superconductivity,[1] two-dimensional conductivity,[2] multiferroicity,[3–8] emergent magnetism,[9–12] and a metal–insulator transition.[13–16] Owing to the close energies and mutual coupling between the lattice, charge, orbital, and spin degrees of freedom in perovskite oxides, their ground-state phases and properties can be modified by applying external perturbations such as electric and magnetic fields, chemical doping, and strain. This strategy can be applied to control the magnetic order by an electric field and so on. For example, recent work on $EuTiO_3$, $SrMnO_3$ (SMO), and $SrCoO_3$ has shown that, under epitaxial strain, the bulk paraelectric (PE) phase can be driven to a ferroelectric (FE) phase accompanied with a change in the magnetic order.[4–6]

In the ideal cubic structure of ABO_3 perovskite compounds, the energy can be tuned by certain distortions such as the polar distortion responsible for the FE ground state and a non-polar antiferrodistortion induced by oxygen octahedral rotation.[17] These distortions can yield complex phase diagrams with intriguing electrical and magnetic properties.[18] With the development of technology for the preparation of epitaxial thin films, the epitaxial growth of heterojunctions and superlattices has become an important strategy for manipulating the structural distortion and modifying the electrical and magnetic properties. A superlattice provides an attractive pathway to create new 'interfacially engineered' materials that do not exist as bulk materials.[19] For example, the artificial $PbTiO_3/SrTiO_3$ superlattice, which has intrinsic ferroelectricity and paraelectricity, can exhibit improper ferroelectricity.[19] Hence, tailoring the functionality of existing materials by selecting an appropriate artificial superlattice system is of great significance.

Here, we focus on the ground-state phases of magnetic perovskite SMO/$BaMnO_3$ (BMO) superlattices and the effects of strain on these phases. Bulk SMO has a cubic perovskite structure, and its magnetic order is G-type antiferromagnetic (G-AFM) below $T_N \sim 260$ K.[20] Previous theoretical research predicted large spin–phonon coupling in SMO; that is, the lowest-frequency polar phonon will dramatically change when the magnetic order changes from G-AFM to the higher-energy ferromagnetic (FM) order. Moreover, it can be driven into a FM–FE multiferroic state by epitaxial strain, and large mixed magnetic–electric–elastic responses have also been predicted in the vicinity of the phase boundary.[5] In addition, recent experiments have shown that an electric polarisation can be induced by doping SMO with Ba ions,[21–25] where the lattice constants are increased by the substitution of larger Ba ions. This result indicates that a tensile strain may also drive the transition from a PE phase to an FE phase. For bulk BMO, the energy of the perovskite structure is higher than that of the hexagonal structure. However, recent theoretical research has revealed that the hypothetical perovskite structure possesses ferroelectricity without any epitaxial strain or chemical doping. Moreover, the perovskite structure can be in the ground state when an epitaxial tensile strain is imposed.[26] Therefore, it is expected that the combination of SMO and BMO in a superlattice is likely

[a]*School of Physical and Technology, National Demonstration Center for Experimental Physics Education, Henan Normal University, Henan Key Laboratory of Photovoltaic Materials, Xinxiang 453007, China. E-mail: jfwang@htu.edu.cn*

[b]*Department of Physics, China University of Mining and Technology, Xuzhou 221116, China*

to induce ferroelectricity and exhibit a wide variety of electrical and magnetic properties under epitaxial strain.

In this study, we systematically investigated the ground-state phases of and the effects of an epitaxial strain on an artificial SMO/BMO superlattice by first-principles calculations. Our results show that the SMO/BMO superlattice has a tetragonal structure (*P4mm* space group) and A-type AFM order and confirm the presence of ferroelectricity. A small tensile strain can transform the ground state into another FE–AFM phase (*Amm*2 space group) with a change in the direction of the ferroelectric polarisation, and a subsequent FE–FM phase with the same symmetry can be obtained with an increase in the tensile strain. In contrast, the system transitions to an FM metal phase under a compressive strain.

II. Computational methods

We performed first-principles calculations using the projector augmented wave (PAW)[27] Vienna *Ab initio* Simulation Package (VASP) code[28,29] with the generalised gradient approximation (GGA) + U method[30] with the Perdew–Becke–Ernzerhof (PBE)[31] parameterisation, an energy cutoff of 600 eV for the plane-wave expansion, and $5 \times 5 \times 5$ K-point Brillouin-zone sampling within a $\sqrt{2} \times \sqrt{2} \times 2$ unit cell (a stacked structure consisting of 1 unit cell of SMO and 1 unit cell of BMO along the c direction, which contains 20 atoms). The energy cutoff and K points were thoroughly tested for convergence. We used the Dudarev implementation[32] with the on-site Coulomb interaction U = 2.5 eV and the on-site exchange interaction $J_H = 1.0$ eV to treat the localised d-electron states in Mn. Each self-consistent electronic calculation converged to 10^{-6} eV, and the tolerance force was set to be 0.005 eV Å^{-1} for ionic relaxation. The calculated equilibrium lattice constant for SMO is 3.845 Å, and the magnetic moment is 2.7μ_B for Mn ions (G-AFM), which is close to the values reported in previous experimental and theoretical studies.[5,20] To simulate the epitaxial strain effects on the SMO/BMO superlattices, we utilised the 'strain-bulk' method.[33,34] With the Berry-phase method,[35] we calculated the FE polarisations for the relaxed structures at the given strain e. By calculating the different energies of states with FM, G-AFM, chain-type antiferromagnetic (C-AFM), and interplane antiferromagnetic (A-AFM) orders, we obtained the in-plane and out-of-plane nearest neighbour coupling exchange constants and then estimated the Curie or Néel temperature at the given e by applying mean field theory.

III. Results and discussions

First, the calculated equilibrium lattice constants of the *P4/mmm* structure for SMO/BMO superlattices with G-AFM and FM orders are a = 3.901 and 3.918 Å, respectively. It is 1.4% larger than that of bulk SMO (G-AFM, 3.845 Å) and may be related to the larger radius of a Ba ion.[26] To determine the phase diagram of SMO/BMO superlattices, we followed the method used by Bousquet *et al.*[19] We started from the prototype PE structure with the *P4/mmm* space group and then identified the instabilities of the highest achievable symmetry by inspection of the phonon dispersion curves. According to the unstable mode of the structure, we lowered the symmetry and performed new structural relaxations. This was repeated until there were no instabilities present. The frequencies of the high-symmetry *P4/mmm* space group with the reference structures with FM and G-AFM orders were computed using frozen phonon methods[36] in a $\sqrt{2} \times \sqrt{2} \times 2$ supercell at the Γ and M points of the primitive perovskite Brillouin zone. The results are listed in Table 1, from which two main results can be concluded. First, we can clearly see that there is strong spin–lattice coupling from the dramatic change in the phonon frequency with magnetic order (FM and G-AFM) in SMO/BMO superlattices. Second, from the presence of unstable modes (both the Γ and M modes, corresponding to polar distortion and octahedral rotation, respectively), we can conclude that the computed high-symmetry *P4/mmm* structure is not in the ground state. The dominant unstable G ($\Gamma_5^-$and Γ_3^-) modes can reduce the symmetry of the *P4/mmm* structure and produce a new state, which has a relatively lower energy compared with the former. For the G-AFM order, it is found that the energies gained from the Γ_3^- and Γ_5^- modes are 4.5 meV f.u.$^{-1}$ and 8.1 meV f.u.$^{-1}$ respectively. These two modes can drive the *P4/mmm* structure to the *P4mm* and *Amm*2 structures (see Fig. 1(a) and (b)). As for the FM order, the energy gains from the Γ_3^- and Γ_5^- modes are up to 82.0 meV f.u.$^{-1}$ and 67.6 meV f.u.$^{-1}$ (see Fig. 2(a)). Obviously, the energy gains of the FM order are much greater than those of the G-AFM order. Owing to this large energy difference, the FM structure will become a possible ground state at a certain strain. Fig. 1(c) and (d) display the M_2^+ and M_5^- modes, indicating that the *P4/mmm* structure can transform into the *P4/mbm* and *Pmma* structures by atomic motion. On the basis of the above analysis, the following structures will be discussed in detail: *P4/mmm*, *P4mm* (Γ_3^-), *P4/mbm* (M_2^+), *P4bm* (Γ_3^- + M_2^+), *Pmma* (M_5^-), *Pma*2 (M_5^- + Γ_3^-), *Pmc*2$_1$ (M_5^- + M_2^+, M_5^- + Γ_5^-, M_5^- + M_2^+ + Γ_5^-), *Amm*2 (Γ_5^-), and *Pc* (M_5^- + M_2^+ + Γ_3^-, M_5^- + M_2^+ + Γ_3^- + Γ_5^-).

For the structures of SMO/BMO superlattices mentioned above with different magnetic orders (FM, A-AFM, C-AFM, and G-AFM), the variations in their total energies of as a function of the epitaxial strain e from −1.31% (compressive) to +3.82% (tensile) are presented in Fig. 3. One can clearly see that there are three possible ground states in the phase diagram: the *P4mm* structure with A-AFM order, the *Amm*2 structure with C-AFM order, and the *Amm*2 structure with FM order. It is noted that the magnetic moment of the FM *Amm*2 phase is 6μ_B f.u.$^{-1}$. The phase boundaries of the lowest energy states are located at e = +0.52% and +1.90%. Moreover, when e < −1.31%, the energy of the *P4mm* (A-AFM) structure is about 8 meV higher (at e =

Table 1 Calculated lowest phonon frequencies of SMO/BMO superlattices with the *P4/mmm* structure at the calculated equilibrium lattice constants with FM and G-AFM orders for high-symmetry q points, which include Γ and M. All values have units of terahertz

	Γ_5^-[110]	Γ_3^-[001]	M_5^-[110]	M_2^+[001]
FM (3.918 Å)	6.788i	6.039i	1.969i	0.623i
G-AFM (3.901 Å)	5.266i	4.624i	2.908	3.468

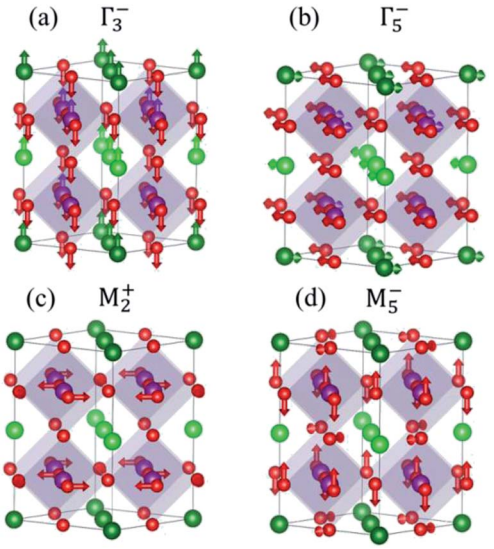

Fig. 1 Schematics of prototype *P*4/*mmm* unit cells of 1/1 SMO/BMO superlattices and the atomic motions associated with the different modes listed in Table 1 (represented by the arrows): (a) Γ_3^- (out-of-plane) mode giving rise to a polarisation along the [001] direction, (b) Γ_5^- (in-plane) mode giving rise to a polarisation along the [110] direction, (c) M_2^+ mode with oxygen octahedral rotation along the [001] axis (out-of-phase), (d) M_5^- mode with oxygen octahedral rotation along the [110] axis (in-phase). The green, olive, magenta, and red spheres represent Sr, Ba, Mn, and O atoms, respectively.

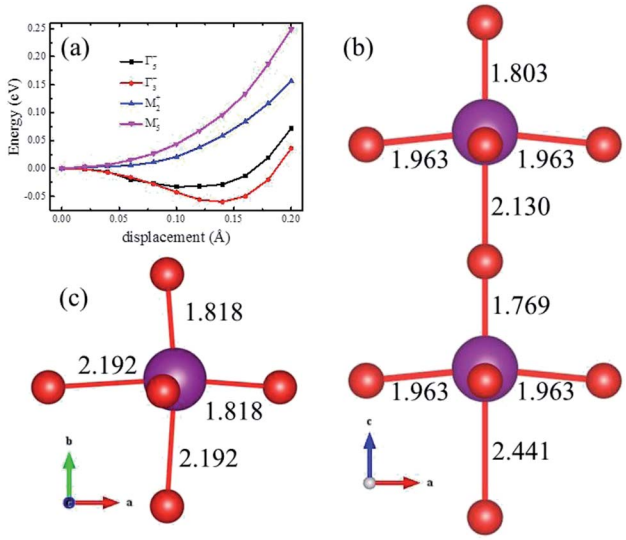

Fig. 2 (a) Evolution of the total energy (per 20-atom unit cell) as a function of the displacement with the unstable modes listed in Table 1 for the *P*4/*mmm* structure with FM order. (b) Mn–O bonds of the relaxed *P*4*mm* structure at $e = -0.77\%$ Å with A-AFM order. (c) Mn–O bonds of the relaxed *Amm*2 structure at $e = +2.43\%$ with FM order.

−1.95%) than that of the *P*4*mm* (FM) structure, which is not shown in Fig. 3. The other calculated structures also end up with these three ground-state structures after the initial structures are fully relaxed. For example, the *P*4*bm* and *Pma*2 structures will end up with the *P*4*mm* structure, the *Pmma* and *P*4/*mbm* structures will end up with the *P*4/*mmm* structure, and the

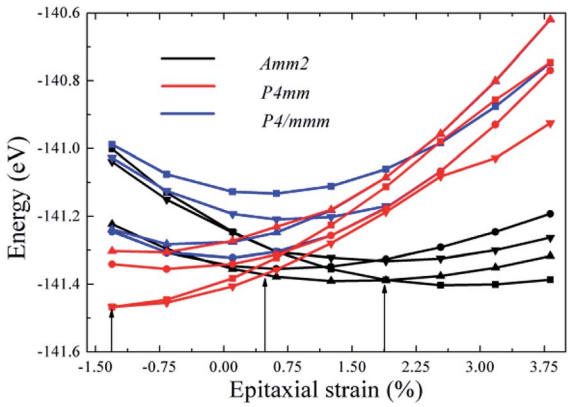

Fig. 3 Total energies of various structures obtained with the GGA + *U* method labelled by the space groups mentioned in the main text. The epitaxial strain (*e*) is defined with respect to the equilibrium lattice constant of the SMO/BMO superlattice with G-AFM magnetic order (3.901 Å), which is close to the equilibrium lattice constant of the *P*4/*mmm* structures with FM and AFM orders. The energies of the structures with FM, G-AFM, C-AFM, and A-AFM orders are indicated by the squares, filled circles, triangles pointing up, and triangles pointing down. The vertical black arrows at $e = -1.31\%$, +0.52%, and +1.90% indicate the phase boundaries. FE_z and FE_{xy} represent the directions of FE polarisation.

Pmc2_1 and *Pc* structures will end up with the *Amm*2 structure. From Fig. 2(a), one can clearly observe that the M modes cannot lower the energy of the *P*4/*mmm* structure; thus, it is not surprising that the M modes are absent for the lowest energy structures after the initial structures (even the initial structures with M modes) are fully relaxed. All of the possible ground states displayed in Fig. 3 combine polar distortions (the [001] direction for the *P*4*mm* structure and the [110] direction for the *Amm*2 structure) with an insulator in our study. This epitaxial-strain-induced ferroelectricity is analogous to that previously observed for artificial $PbTiO_3/SrTiO_3$ superlattices with the *P*4*bm* ([001] direction) and *Pmc*2_1 ([110] direction) structures.[19] Here, we should emphasise that compared with SMO thin films,[5] the SMO/BMO superlattice retains multiferroic properties regardless of whether or not an epitaxial strain is applied; hence, it should be easier to realise in experiments. To further understand the origin of ferroelectricity, the lengths of the Mn–O bonds in the *P*4*mm* (A-AFM) and *Amm*2 (FM) structures are shown in Fig. 2. We can clearly see that the Mn ions are displaced from the centre of an O octahedron. For the *P*4*mm* structure, the Mn ions are displaced along the [001] direction. In contrast, for the *Amm*2 structure, they are displaced along the [110] direction. These displacements of Mn ions are the origin of the FE polarisation. Another interesting fact is the magnetic phase transition from C-AFM to FM at $e = +1.9\%$ for the *Amm*2 structure. This may be attributed to the large deviation in the Mn–O–Mn bond angles from 180° with the increase in tensile strain, which weakens the AFM t_{2g}–t_{2g} superexchange and introduces an FM double perovskite *via* enhanced Mn e_g–O p hybridisation.[5,23,37] This large deviation is caused by the enhanced polar distortion, as is reflected in the increase in the FE polarisation with the increase in tensile strain (Fig. 4).

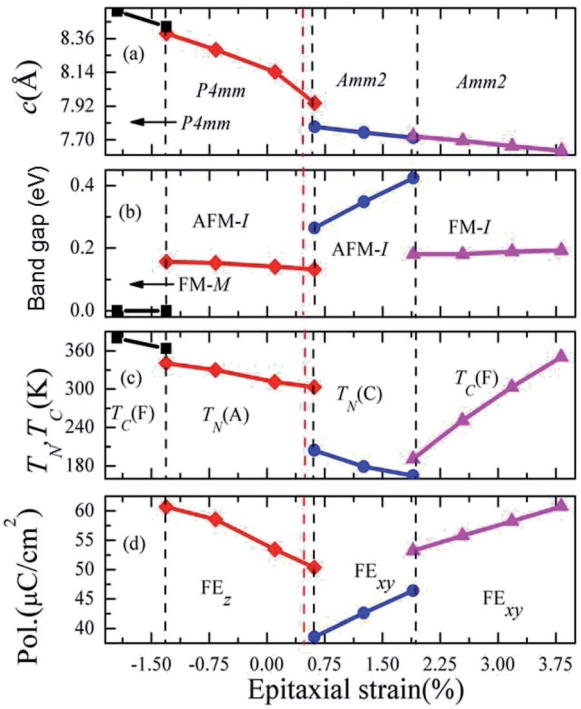

Fig. 4 Properties of SMO/BMO superlattices as a function of the epitaxial strain computed using the GGA + *U* method: (a) lattice parameter *c* for the possible ground state at each strain value, (b) band gap, (c) critical temperatures for magnetic order estimated by the mean field method, and (d) FE polarisation of the lowest energy structure. The red dashed lines represent the phase boundary between the *P4mm* structure with A-AFM order and the *Amm*2 structure with C-AFM order. The symbols are shown in Fig. 3.

In Fig. 4(a)–(d), we present the lattice parameter *c*, band gap, critical temperatures (T_C and T_N), and FE polarisation within the range of strain from −1.95% to +3.82%. As the strain increases, there are jumps in *c* at $e = -1.31\%$ (from the ferromagnetic metal (FM-M) phase to the antiferromagnetic-insulator-ferroelectric (AFM-I-FE$_z$) phase) and $e = +0.52\%$ (from the AFM-I-FE$_z$ phase to the AFM-I-FE$_{xy}$ phase), as displayed in Fig. 4(a). These jumps in *c* lattice constant have a close correlation with the phase transition. For example, the ferroelectric polarization of the AFM-FE$_z$ phase has a positive correlation with the *c* lattice constant, and the ferroelectric polarization of the *Amm*2 phases have a negative correlation with the *c* lattice constant, as shown in Fig. 4(a) and (d). In Fig. 4(b), we can see that the AFM insulating phase can be transformed into FM metal phase at $e = -1.31\%$. This indicates that an insulator–metal transition will occur in the vicinity of the phase boundary when a suitable compressive strain is applied. In addition, the band gap of the AFM-I (*Amm*2) state is larger than other insulating phases (AFM-I and FM-I) and increases with increasing epitaxial strain. The critical temperatures for magnetic order calculated by mean field method are shown in Fig. 4(c). The critical temperatures of both the FM (T_C) and A-AFM (*P4mm*) (T_N) phases are above room temperature. The T_C of the FM phase (*Amm*2) is above 190 K at $e = +1.90\%$ and increases with increasing *e*. Taking the centrosymmetric phase as the reference state (*Pnma* structure), we calculated the electric polarisations of the three FE phases of SMO/BMO superlattices, as shown in Fig. 4(d). Within the range of epitaxial strain, both the AFM (*P4mm*) phase at $e = -1.31\%$ and FM (*Amm*2) at $e = +3.75\%$ exhibit a highest electric polarisation of 61 μC cm^{-2}. The AFM (*P4mm*) phase shows an improved electric polarisation with decreasing the epitaxial strain ($e \leq +0.52\%$), but the electric polarisation of both AFM (*Amm*2) and FM (*Amm*2) phases increase with increasing the tensile epitaxial strain ($e \geq +0.52\%$). It indicates that a slight tensile epitaxial strain can drive AFM (*P4mm*) phase to AFM (*Amm*2) phase, this may has a relationship with the change of the ferroelectric polarisation from an out-of-plane direction to an in-plane direction. It is should be noted that there are large jumps in magnetic, electric, and elastic properties across the phase boundaries. First, at −1.31%, the two phases in the vicinity of the phase boundary are FM-M and AFM-I-FE$_z$. Second, at +0.52%, the two phases are AFM-I-FE$_z$ and AFM-I-FE$_{xy}$. These two phases have different values of *c* (Fig. 4(a)) and different directions and magnitudes of the electric polarisation (Fig. 4(d)). Third, at +1.90%, the two phases are AFM-I-FE$_{xy}$ and FM-I-FE$_{xy}$. Based on the above discussions, one can expect a strong magnetic–electrical coupling to exist in the vicinity of the phase boundary, since applying external perturbations such as electric or magnetic field tends to drive a phase transition due to the close energy between two phases.[5,12,19]

IV. Conclusions

In summary, we have investigated the spin–phonon coupling and the effects of the strain on the ground-state phases of layered SMO/BMO superlattices by first-principles calculations. The main results show that this system has AFM order and an intrinsic FE polarisation with the *P4mm* space group. A tensile epitaxial strain can drive the ground state to another AFM–FE phase and then to a FM–FE phase with the *Amm*2 space group with a large electric polarisation (>53 μC cm^{-2}) and magnetisation ($6\mu_B$ f.u.$^{-1}$), accompanied by a change in the FE polarisation from an out-of-plane direction to an in-plane direction. In contrast, a compressive uniaxial stress applied to the FM-M phase could induce a metal–insulator transition.

Conflicts of interest

There are no conflicts to declare.

Acknowledgements

This work was supported by the National Natural Science Foundation of China (No. U1504107 and 11447129) and the Doctoral Scientific Research Foundation (qd15214).

References

1 N. Reyren, S. Thiel, A. D. Caviglia, L. F. Kourkoutis, G. Hammerl, C. Richter, C. W. Schneider, T. Kopp, A. S. Ruetschi, D. Jaccard, M. Gabay, D. A. Muller, J. M. Triscone and J. Mannhart, *Science*, 2007, **317**, 1196.

2 A. Ohtomo, D. A. Muller, J. L. Grazul and H. Y. Hwang, *Nature*, 2002, **419**, 378.
3 D. Doennig, W. E. Pickett and R. Pentcheva, *Phys. Rev. Lett.*, 2013, **111**, 126804.
4 J. H. Lee, L. Fang, E. Vlahos, X. Ke, Y. W. Jung, L. F. Kourkoutis, J.-W. Kim, P. J. Ryan, T. Heeg, M. Roeckerath, V. Goian, M. Bernhagen, R. Uecker, P. C. Hammel, K. M. Rabe, S. Kamba, J. Schubert, J. W. Freeland, D. A. Muller, C. J. Fennie, P. Schiffer, V. Gopalan, E. Johnston-Halperin and D. G. Schlom, *Nature*, 2010, **466**, 954.
5 J. H. Lee and K. M. Rabe, *Phys. Rev. Lett.*, 2010, **104**, 207204.
6 J. H. Lee and K. M. Rabe, *Phys. Rev. Lett.*, 2011, **107**, 067601.
7 G. Song and W. Zhang, *Sci. Rep.*, 2014, **4**, 4564.
8 S. R. Spurgeon, P. V. Balachandran, D. M. Kepaptsoglou, A. R. Damodaran, J. Karthik, S. Nejati, L. Jones, H. Ambaye, V. Lauter, Q. M. Ramasse, K. K. S. Lau, L. W. Martin, J. M. Rondinelli and M. L. Taheri, *Nat. Commun.*, 2015, **6**, 6735.
9 M. Salluzzo, S. Gariglio, D. Stornaiuolo, V. Sessi, S. Rusponi, C. Piamonteze, G. M. De Luca, M. Minola, D. Marré, A. Gadaleta, H. Brune, F. Nolting, N. B. Brookes and G. Ghiringhelli, *Phys. Rev. Lett.*, 2013, **111**, 087204.
10 N. Ganguli and P. J. Kelly, *Phys. Rev. Lett.*, 2014, **113**, 127201.
11 S. Banerjee, O. Erten and M. Randeria, *Nat. Phys.*, 2013, **9**, 626.
12 J. T. Heron, J. L. Bosse, Q. He, Y. Gao, M. Trassin, L. Ye, J. D. Clarkson, C. Wang, J. Liu, S. Salahuddin, D. C. Ralph, D. G. Schlom, J. Iniguez, B. D. Huey and R. Ramesh, *Nature*, 2014, **516**, 370.
13 R. Scherwitzl, S. Gariglio, M. Gabay, P. Zubko, M. Gibert and J. M. Triscone, *Phys. Rev. Lett.*, 2011, **106**, 246403.
14 J. Y. Zhang, C. A. Jackson, R. Chen, S. Raghavan, P. Moetakef, L. Balents and S. Stemmer, *Phys. Rev. B: Condens. Matter Mater. Phys.*, 2014, **89**, 075140.
15 J. Y. Zhang, J. Hwang, S. Raghavan and S. Stemmer, *Phys. Rev. Lett.*, 2013, **110**, 256401.
16 P. Di Pietro, J. Hoffman, A. Bhattacharya, S. Lupi and A. Perucchi, *Phys. Rev. Lett.*, 2015, **114**, 156801.
17 X. Zhai, L. Cheng, Y. Liu, C. M. Schlepütz, S. Dong, H. Li, X. Zhang, S. Chu, L. Zheng, J. Zhang, A. Zhao, H. Hong, A. Bhattacharya, J. N. Eckstein and C. Zeng, *Nat. Commun.*, 2014, **5**, 4283.
18 H. Y. Hwang, Y. Iwasa, M. Kawasaki, B. Keimer, N. Nagaosa and Y. Tokura, *Nat. Mater.*, 2012, **11**, 103.
19 E. Bousquet, M. Dawber, N. Stucki, C. Lichtensteiger, P. Hermet, S. Gariglio, J.-M. Triscone and P. Ghosez, *Nature*, 2008, **452**, 732.
20 T. Takeda and S. Ōhara, *J. Phys. Soc. Jpn.*, 1974, **37**, 275.
21 H. Chen and A. J. Millis, *Phys. Rev. B*, 2016, **94**, 165106.
22 H. Sakai, J. Fujioka, T. Fukuda, D. Okuyama, D. Hashizume, F. Kagawa, H. Nakao, Y. Murakami, T. Arima, A. Q. R. Baron, Y. Taguchi and Y. Tokura, *Phys. Rev. Lett.*, 2011, **107**, 137601.
23 G. Giovannetti, S. Kumar, C. Ortix, M. Capone and J. van den Brink, *Phys. Rev. Lett.*, 2012, **109**, 107601.
24 N. Ogawa, Y. Ogimoto, Y. Ida, Y. Nomura, R. Arita and K. Miyano, *Phys. Rev. Lett.*, 2012, **108**, 157603.
25 R. Nourafkan, G. Kotliar and A. M. S. Tremblay, *Phys. Rev. B: Condens. Matter Mater. Phys.*, 2014, **90**, 220405.
26 J. M. Rondinelli, A. S. Eidelson and N. A. Spaldin, *Phys. Rev. B: Condens. Matter Mater. Phys.*, 2009, **79**, 205119.
27 P. E. Blöchl, *Phys. Rev. B: Condens. Matter Mater. Phys.*, 1994, **50**, 17953.
28 G. Kresse and J. Hafner, *Phys. Rev. B: Condens. Matter Mater. Phys.*, 1993, **47**, 558.
29 G. Kresse and J. Furthmüller, *Phys. Rev. B: Condens. Matter Mater. Phys.*, 1996, **54**, 11169.
30 C. Loschen, J. Carrasco, K. M. Neyman and F. Illas, *Phys. Rev. B: Condens. Matter Mater. Phys.*, 2007, **75**, 035115.
31 J. P. Perdew, K. Burke and M. Ernzerhof, *Phys. Rev. Lett.*, 1996, **77**, 3865.
32 S. L. Dudarev, G. A. Botton, S. Y. Savrasov, C. J. Humphreys and A. P. Sutton, *Phys. Rev. B: Condens. Matter Mater. Phys.*, 1998, **57**, 1505.
33 N. A. Pertsev, A. G. Zembilgotov and A. K. Tagantsev, *Phys. Rev. Lett.*, 1998, **80**, 1988.
34 O. Diéguez, K. M. Rabe and D. Vanderbilt, *Phys. Rev. B: Condens. Matter Mater. Phys.*, 2005, **72**, 144101.
35 R. D. King-Smith and D. Vanderbilt, *Phys. Rev. B: Condens. Matter Mater. Phys.*, 1993, **47**, 1651.
36 A. Togo, F. Oba and I. Tanaka, *Phys. Rev. B: Condens. Matter Mater. Phys.*, 2008, **78**, 134106.
37 M. Astrid, F. Carina, A. Ulrich, N. A. Spaldin and S. M. Selbach, *MRS Commun.*, 2016, **6**, 182.